Direct single-molecule observation of calcium-dependent misfolding in human neuronal calcium sensor-1

Pétur O. Heidarsson[a], Mohsin M. Naqvi[b,c], Mariela R. Otazo[b,d], Alessandro Mossa[e], Birthe B. Kragelund[a,1], and Ciro Cecconi[b,c,1]

[a]Structural Biology and NMR Laboratory, Department of Biology, University of Copenhagen, 2200 Copenhagen, Denmark; [b]Institute of Nanoscience S3, Consiglio Nazionale delle Ricerche, 41125 Modena, Italy; [c]Department of Physics, Informatics and Mathematics, University of Modena and Reggio Emilia, 41125 Modena, Italy; [d]Department of Physics, Center of Applied Technologies and Nuclear Development, Havana, Cuba; and [e]Department of Physics, University of Bari and Istituto Nazionale di Fisica Nucleare, Sezione di Bari, 70126 Bari, Italy

Edited by Martin Gruebele, University of Illinois at Urbana-Champaign, Urbana, IL, and approved August 8, 2014 (received for review February 5, 2014)

Neurodegenerative disorders are strongly linked to protein misfolding, and crucial to their explication is a detailed understanding of the underlying structural rearrangements and pathways that govern the formation of misfolded states. Here we use single-molecule optical tweezers to monitor misfolding reactions of the human neuronal calcium sensor-1, a multispecific EF-hand protein involved in neurotransmitter release and linked to severe neurological diseases. We directly observed two misfolding trajectories leading to distinct kinetically trapped misfolded conformations. Both trajectories originate from an on-pathway intermediate state and compete with native folding in a calcium-dependent manner. The relative probability of the different trajectories could be affected by modulating the relaxation rate of applied force, demonstrating an unprecedented real-time control over the free-energy landscape of a protein. Constant-force experiments in combination with hidden Markov analysis revealed the free-energy landscape of the misfolding transitions under both physiological and pathological calcium concentrations. Remarkably for a calcium sensor, we found that higher calcium concentrations increased the lifetimes of the misfolded conformations, slowing productive folding to the native state. We propose a rugged, multidimensional energy landscape for neuronal calcium sensor-1 and speculate on a direct link between protein misfolding and calcium dysregulation that could play a role in neurodegeneration.

protein folding | NCS-1 | off-pathway intermediate | conformational dynamics | optical trapping

Most proteins have evolved to fold rapidly into a specific and functional 3D structure immediately after translation from the ribosome. The folding process is, however, not adequately efficient to prevent the occurrence of misfolded states in vivo (1), especially in the case of larger multidomain proteins which comprise roughly 75% of the human proteome (2, 3). Normally, to tackle and destroy these unproductive structures, cells are equipped with competent clean-up machinery, such as chaperones, proteasomes, and unfoldases (4). If misfolding cannot be ameliorated, these nonnative states accumulate in the cell to form aggregates with potential pathophysiological consequences (5).

The emerging view that protein misfolding is a common phenomenon in living cells is still largely unsubstantiated, as detecting and characterizing misfolded states has been experimentally challenging (2, 6). The mechanistic details that have accumulated over the last decades on misfolding have mostly come from studies on the resulting oligomeric structures and amyloid formation (1), whereas our understanding of the structural rearrangements and pathways leading to precursory misfolded states is still highly incomplete. Importantly, the formation of prefibrillar monomeric and oligomeric misfolded states is, contrary to amyloids, reversible and thus these states provide a potential target for drug design.

Sparse populations and their associated weak signals limit the use of traditional bulk methods for monitoring the early events of misfolding, and relatively few systems have been studied in detail (7–13). Now, single-molecule force spectroscopy techniques, such as optical tweezers, enable detection of rare alternative folding pathways and short-lived misfolded states by direct mechanical manipulation (14–19). Although aggregation requires more than one molecule, nonnative structural rearrangements within a single molecule only report on monomeric misfolded states. Recent works have exploited these properties to study misfolding of well-known disease-related proteins, such as the prion protein, as well as proteins not generally associated with misfolding, such as the EF-hand calcium sensor calmodulin (CaM) (20–22).

The EF-hand superfamily of calcium sensors is responsible for translating changing levels of intracellular Ca^{2+} concentration into a biochemical signal through conformational changes that allow them to interact with an array of binding targets (23). The subfamily of neuronal calcium sensors (NCS) is mostly expressed in neurons and currently includes 15 members (24, 25). Neuronal calcium sensor-1 (NCS-1) is the most ancient member of this family (Fig. 1*A*), and it has been functionally associated with

Significance

Protein misfolding can lead to neurodegeneration. Yet, the mechanistic details of this deleterious phenomenon are largely unknown, as experimental portrayals of the early and reversible molecular events leading to misfolded conformations have so far remained highly limited. Here we use single-molecule optical tweezers to monitor the structural rearrangements leading to misfolded conformations of human neuronal calcium sensor-1, a protein linked to serious neurological disorders. We identified two distinct and calcium-dependent misfolding trajectories originating from an on-pathway folding intermediate. Remarkably for a calcium sensor, pathologically high calcium concentrations impede correct folding by increasing the occupation probabilities of the misfolded states. The results open ostensible links between protein misfolding and calcium dysregulation that could be important in neurodegeneration and its potential inhibition.

Author contributions: P.O.H., M.R.O., B.B.K., and C.C. designed research; P.O.H., M.M.N., and M.R.O. performed research; A.M. contributed new reagents/analytic tools; P.O.H., M.M.N., M.R.O., A.M., B.B.K., and C.C. analyzed data; and P.O.H., M.M.N., A.M., B.B.K., and C.C. wrote the paper.

The authors declare no conflict of interest.

This article is a PNAS Direct Submission.

Freely available online through the PNAS open access option.

[1]To whom correspondence may be addressed. Email: ciro.cecconi@gmail.com or bbk@bio.ku.dk.

This article contains supporting information online at www.pnas.org/lookup/suppl/doi:10.1073/pnas.1401065111/-/DCSupplemental.

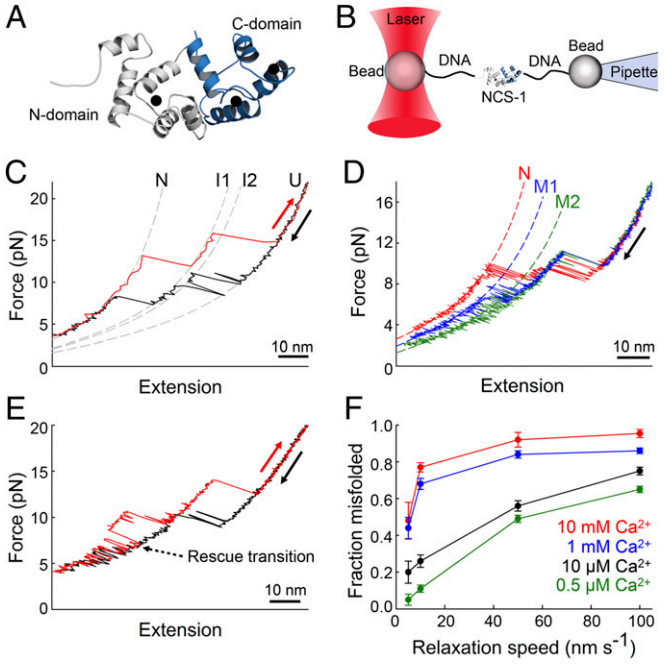

Fig. 1. Misfolding pathways of NCS-1. (*A*) The NMR structure of NCS-1 (PDB 2LCP), with the N domain (EF1/EF2) depicted in gray and the C domain (EF3/EF4) in blue. Black spheres represent Ca^{2+} ions. EF1 does not bind Ca^{2+} because of a conserved cysteine-proline mutation (35). (*B*) Sketch of the experimental setup. NCS-1 was tethered between functionalized beads via DNA handles and stretched and relaxed by moving the pipette relative to the optical trap (16, 62). (*C*) Native folding pathway of NCS-1. After being mechanically stretched and unfolded (red trace), NCS-1 refolds upon relaxation of the applied force into its native state via two intermediate states, I1 and I2. Dashed lines are worm-like-chain fits to the data. Color-coded arrows indicate the pulling/relaxing directions. (*D*) Misfolding pathways of NCS-1. During refolding, NCS-1 sometimes follows alternative pathways leading to misfolded states M1 (blue) or M2 (green), which are less compact than the native state (red). Dashed lines are worm-like-chain fits to the data. (*E*) Rescue of the native state of NCS-1. During relaxation (black), the molecule misfolded. During stretching (red), nonnative contacts of the misfolded conformation are progressively broken, until the molecule can find its native folding pathway ("rescue transition"). (*F*) Fraction of folding pathways leading to either M1 or M2 as a function of Ca^{2+} concentration and relaxation speed. Higher Ca^{2+} concentrations and relaxation speeds facilitate NCS-1 misfolding. Error bars indicate SEs of mean. At least five different molecules were used for each calcium concentration.

cognitive processes, such as learning and memory (26, 27), and with a number of cellular processes such as neurotransmitter release (28, 29), and regulation of ion channels, and G protein coupled receptors (GPCRs) (24, 30), including the dopamine receptor D2 (31). NCS-1 has also been linked to serious neurodegenerative disorders including schizophrenia, bipolar disorder (BD) (32), and autism (33, 34). However, the dysfunctions of NCS-1 are poorly characterized on the molecular level, and whether they involve altered functional profiles or loss of function due to formation of misfolded states is currently unknown.

Because only a few systems have been studied experimentally, little is known about folding and/or misfolding mechanisms of members of the EF-hand superfamily (21, 35–37). The extensively studied CaM has been shown on the single-molecule level to frequently visit misfolded states that slow down the overall folding rate of the protein (21). The physiological consequences of CaM misfolding have not yet been explored. NCS-1 shares modest sequence homology with CaM, mostly within and around the calcium binding sites (24). Similar to CaM, NCS-1 contains four EF hands organized in two EF domains (Fig. 1*A*) yet it exhibits a larger number of interdomain contacts (38), a feature that has been suggested to increase the probability of misfolding in proteins (2). The formation of misfolded states along the folding pathway of NCS-1 may have important consequences with regards to its function as a calcium sensor and might also play a role in disease pathologies.

Using optical tweezers, we have recently characterized the native folding pathway of NCS-1 (39). Here we use a similar experimental approach to monitor individual NCS-1 molecules as they populate nonnative misfolded states in real time. We identified two misfolding trajectories leading to two distinct misfolded conformations, characterized by different extensions and different pathways on the energy landscape. Both misfolding pathways originated from a partially folded on-pathway intermediate state, and they competed with native folding. The occupancy probability of both misfolded states could be controlled by modulating either the relaxation rate of the applied force and/or the calcium concentration. Remarkably for a calcium sensor, higher calcium concentrations, even within physiologically relevant conditions, lead to an increased probability of NCS-1 misfolding.

Results

Individual NCS-1 molecules were manipulated with polystyrene beads by means of DNA molecular handles covalently attached to cysteine residues engineered at positions 4 and 188, as previously reported (39) (Fig. 1*B* and *Methods*). To identify and characterize misfolding pathways of NCS-1, we first performed constant-velocity experiments, where the molecule is stretched and relaxed by moving the pipette at constant speed relative to the optical trap (16, 39, 40). Under these experimental conditions, we have previously shown that NCS-1 unfolds in an apparent three-state manner and folds back into its native state through a process that starts with the folding of the C domain, undergoing a major conformational change (U→I2) followed by a minor rearrangement (I2→I1), and ends with the folding of the N domain at lower forces (I1→N transition) (Fig. 1*C*). The I2→I1 transition is the rate-limiting step of the overall folding process and is mandatory for the subsequent folding of the N domain. Here we show that, in addition to the pathway leading to the native state, NCS-1 folding can follow alternative pathways leading to nonnative (misfolded) structures (Fig. 1*D*). In these cases, the protein folds into I2 but fails to transit into I1, thus never reaching the natively structured C domain. At lower forces, the molecule starts fluctuating between I2 and misfolded conformations, before being trapped in either of two main misfolded states, M1 and M2, differentiated by their extension (Fig. 1*D*, green and blue traces). A fit of the force vs. extension traces to the worm-like-chain (WLC) model of polymer elasticity (41) yielded a contour length change (ΔL_c) of 29 ± 2 nm (n = 35; errors are given as SD) for the I2−M1 transition, and ΔL_c = 18 ± 3 nm (n = 31) for the I2−M2 transition. These states are clearly different from the native state as the native I2−I1−N transition has an overall associated contour length change of 34 ± 2 nm (39). Furthermore, M1 and M2 displayed drastically reduced mechanical stability compared with the native state and unfolded at lower forces (Fig. S1). During stretching, kinetically trapped misfolded molecules were occasionally (<1%) observed to snap into their native state through a "rescue transition" that suddenly shortened the extension of the molecule (Fig. 1*E*, red trace). The rescue transition occurred exclusively from I2, not from M1 or M2, and usually nonnative interactions had to be mechanically broken in an unfolding step before the molecule could fold into N, supporting the off-pathway nature of the kinetically trapped conformations. Upon further increase of force, the molecule displayed the signature of high-force unfolding transitions of both the N and C domains, verifying a native fold.

To examine any possible effects of Ca^{2+} concentration and relaxation speed on the misfolding behavior of NCS-1, we performed experiments in 0.5 μM, 10 μM, 1 mM, and 10 mM $CaCl_2$,

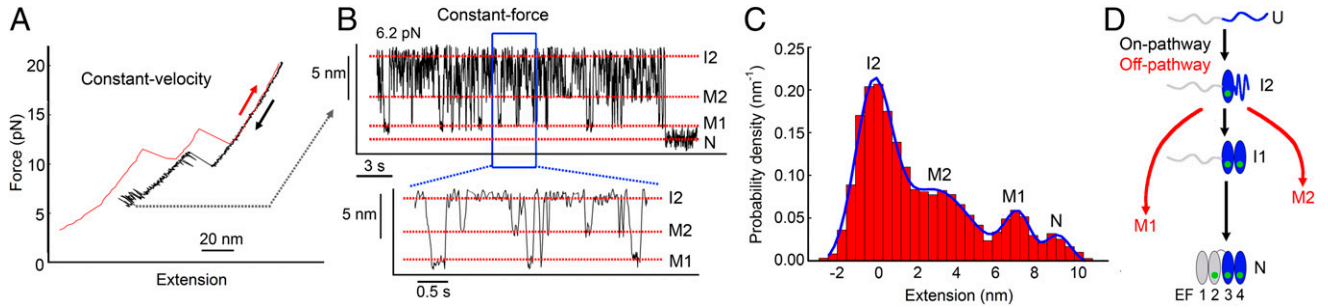

Fig. 2. Misfolding of NCS-1 at equilibrium. (*A*) Force vs. extension cycle showing a mechanically denatured NCS-1 molecule (red trace) that, during relaxation of the applied force, follows a misfolding pathway (black trace). Relaxation was stopped at 6.2 pN, and (*B*) the force was clamped via a feedback mechanism to observe NCS-1 fluctuate at equilibrium between I2 and misfolded states M1 and M2, until it eventually folded into its native state. (*Inset*) A magnified view of the data in the blue box. (*C*) Probability density distribution of the extension values of *B*, resolving misfolded states M2 and M1. The distribution was fit by the sum of four Gaussian functions (blue line) to show that M2 and M1 are located at 3.2 ± 2.4 nm and 7.6 ± 1.1 nm, respectively, from I2. (*D*) Diagram of the different molecular states populated during the folding of NCS-1. Fully folded EF hands are shown as gray or blue ellipses, for the N or C domain, respectively, and Ca^{2+} ions are shown as green circles.

at various relaxation speeds. At all calcium concentrations, the misfolding probability of NCS-1 increased with increasing relaxation speed (Fig. 1*F*). Strikingly, the misfolding probability also increased with increased Ca^{2+} concentration. At a physiologically relevant calcium concentration (0.5 μM) and at slow relaxation speed (5 nm·s^{-1}), only 5% of the molecules misfolded. When the calcium concentration was raised to 10 mM, almost 50% of the molecules misfolded. These data are highly interesting, as various physiological or pathophysiological phenomena can cause a transient or sustained increase in neuronal calcium concentrations (42–44), as further addressed in *Discussion*. The two misfolded states, M1 and M2, were also diversely populated at different Ca^{2+} concentrations (Fig. S2). The M1 state was highly populated at 10 mM Ca^{2+} and less populated at 1 mM Ca^{2+}, whereas it was absent at lower Ca^{2+} concentrations. The M2 state instead was equally populated under all four experimental conditions. Rescuing transitions were observed at all calcium concentrations, and their frequency increased with lower calcium concentrations (~1% at 10 mM to ~5% at 10 μM).

To characterize the kinetics and thermodynamics of the misfolded states, we performed constant-force measurements, both at high (10 mM) and low (10 μM) calcium concentrations. Under both conditions, the calcium concentration is above bulk dissociation constants (4–400 nM) (35), suggesting the calcium binding sites of NCS-1 to be saturated. In these experiments, a molecule was stretched and relaxed multiple times until it was observed to populate a pathway leading to a misfolded state (Fig. 2*A*). At this point, the relaxation of the molecule was stopped and the applied force was clamped via a force-feedback mechanism to a specific tension to observe NCS-1 fluctuate at equilibrium between I2 and misfolded conformations, before eventually folding into N (typically after 20–100 s) (Fig. 2*B*). In all cases (>300 events), the transition to N took place from I2, providing additional evidence for the off-pathway nature of the misfolded states. After the molecule had folded into the native state, it did not unfold again within the measuring time (>5 min). The probability density distribution of the extension signal revealed that in 10 mM Ca^{2+}, NCS-1 primarily populates two misfolded states positioned at 3.2 ± 2.4 nm and 7.6 ± 1.1 nm from I2 (Fig. 2*C*). These extensions compare well to those of the misfolded states M2 and M1 observed in constant-velocity measurements (Fig. 1*D*), suggesting that the most probable nonnative conformations populated by NCS-1 at equilibrium are also the conformations in which it remains kinetically trapped at lower forces. The kinetic network of the on- and off-pathway states of NCS-1 is shown in Fig. 2*D*.

To characterize the energies and transition kinetics of M1 and M2, extension-time traces were recorded at different forces, in the range between 5.4 pN and 7.0 pN. A population shift from I2 to the misfolded states was observed when the applied force was reduced (Fig. 3*A*). The force-dependent rates of the I2–M2 and I2–M1 transitions were subsequently determined by analyzing each extension trace with a hidden Markov model (HMM) algorithm (45–47). Experimental data are well modeled by a four-state Markov system where M1 and M2 are only connected to I2, while the transition from I2 to N (in our force range, the transient occupation of state I1 is too short-lived to be detected) is only one way. The position of the transition states along the reaction coordinate and the zero force rates were then estimated by fitting the data to a linearized form of the Bell model (39, 48)

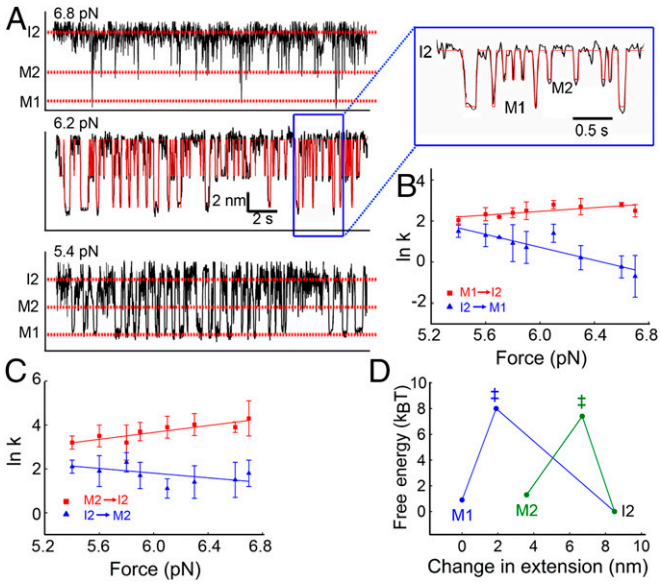

Fig. 3. Energetics and kinetics of NCS-1 misfolding in 10 mM Ca^{2+}. (*A*) Extension vs. time traces of NCS-1 fluctuations at indicated forces. As the force is lowered, the M1 and M2 states are increasingly populated. (*Inset*) A magnified view of the misfolding transitions in the blue box, and the corresponding fit based on the HMM (red line). *B* and *C* show unfolding (red) and refolding (blue) rate constants at different forces for the I2–M1 and I2–M2 transitions, respectively. Solid lines are fits with a linearized form of the Bell model (40, 48). Error bars represent SDs. (*D*) Sketch of the free-energy landscapes for the I2–M2 (green) and I2–M1 (blue) transitions at 5.5 pN and 10 mM Ca^{2+}, reconstructed using the HMM analysis. The I2 state was considered the reference state at zero energy.

(Fig. 3 *B* and *C*). From the position of the transition states, we deduced a difference in extension of 4.9 ± 1.3 nm between I2 and M2, and of 8.4 ± 1.3 nm between I2 and M1 (Table 1). These distances compare well with the observed jumps of the extension in the recorded traces (Fig. 2*B* and Fig. S3), showing the overall consistency of our HMM reconstruction. The dwell time distributions of I2, M1, and M2 determined from the HMM analysis could be well fit to single exponentials, which is compatible with a two-state behavior of the transitions among these states (Fig. S3). From the rates, the salient features of the energy landscapes for the I2−M1 and I2−M2 transitions were reconstructed (Fig. 3*D* and Table 1). The height of the free-energy barriers depends on a preexponential factor, which we cannot measure directly with our instrument. We adopted the value 1.2×10^4 Hz that has been recently measured with a similar setup (49).

In constant-force experiments and low calcium concentration (10 μM Ca^{2+}), in keeping with what was observed in constant-velocity experiments (Fig. S2), NCS-1 populated only the misfolded state M2 (Fig. 4*A*), although very rare excursions to a state resembling M1 has been observed. Here the best reconstruction was obtained by positing a three-state Markov model with forbidden transitions between M2 and N. Our HMM analysis (Fig. 4*B*) yielded distances to the transition state for the I2−M2 transition that sum to 4.2 ± 0.8 nm (Table 1), in good agreement with the observed jumps of the extension in the recorded traces (Fig. 4*C* and Figs. S4 and S5). From the rate constants analysis, the energy landscape governing the I2−M2 transition was reconstructed (Fig. 4*D*), showing that at low calcium, the I2 to M2 transition has an activation energy quite similar to that observed at 10 mM Ca^{2+}. These data are consistent with the weak Ca^{2+} dependence of the occupancy probability of M2 observed in constant-velocity experiments (Fig. S2).

The impact of varying the calcium concentration on the extent of misfolding suggests that one or more of the three calcium-binding sites plays a key role in the formation of misfolded states. We therefore separately introduced classical mutations that prevent ion binding into each of the three calcium-binding EF-hand loops (39). Because folding reaches I2 before any misfolding occurs and because previous manipulation of the EF3 binding site disables folding, with no apparent native transitions and with similar behavior to the apo form of NCS-1 (39), this rules out EF3 as the origin for generation of misfolded states. In contrast, variants carrying disabled EF2 (NCS-1^{EF2}) or EF4 (NCS-1^{EF4}) binding sites still retain some native and nonnative folding transitions (39). Importantly, NCS-1^{EF2} never populates M1 or M2, as the C domain always folds properly into its native structure, even at high Ca^{2+} concentrations and relaxation speeds (Fig. S6). This behavior is strikingly different from that of the wild-type NCS-1 that, under the same experimental conditions, fails to natively fold its C domain, and thus misfolds, in ~80% of the cases (Fig. 1*E*). In contrast to NCS-1^{EF2}, NCS-1^{EF4} never transits from I2 to I1, because this transition involves binding of Ca^{2+} to EF4 (39), and thus its C domain never reaches its native conformation. Nonetheless and surprisingly, with NCS-1^{EF4}, we could not detect any transitions from I2 to conformations resembling M1 or M2 (Fig. S6). Instead, at low forces, this variant folded into a structure with an extension significantly larger than those of the misfolded states populated by the wild-type NCS-1. These results collectively allowed us to conclude that both the EF2 and EF4 calcium binding sites are critical in the formation of misfolded states, as highlighted in *Discussion*.

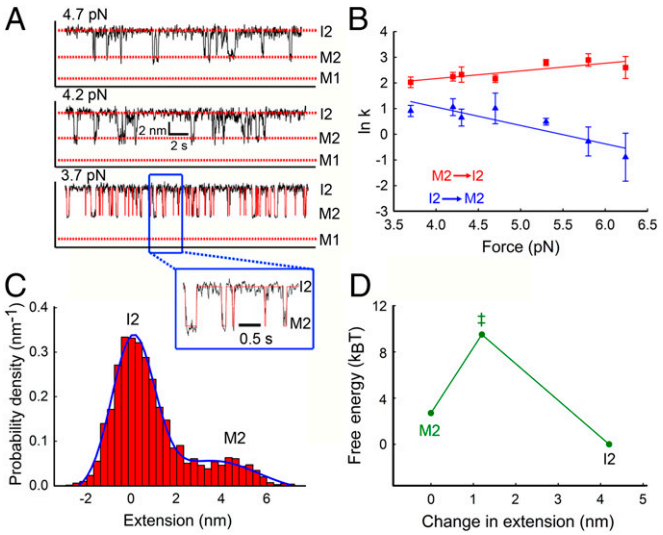

Fig. 4. Energetics and kinetics of NCS-1 misfolding in 10 μM Ca^{2+}. (*A*) Extension vs. time traces of NCS-1 fluctuations at three different forces. An increase in force leads to a decrease in the occupation probability of M2. The expected extension of the M1 state is also indicated. (*Inset*) A magnified view of the misfolding transitions in the blue box and the corresponding fit based on the HMM (red line). (*B*) Unfolding (red) and refolding (blue) rate constants at different forces for the I2−M2 transition as determined from the HMM analysis, and fits with the Bell model (solid lines). Error bars represent SDs. (*C*) Probability density distribution of the extension values of the 3.7 pN trace of *A*. The distribution was fit to a double-Gaussian function showing that M2 is located at 4.0 ± 1.7 nm from I2. (*D*) Sketch of the free-energy landscape for I2−M2 transition at 5.5 pN and 10 μM Ca^{2+}, reconstructed using the HMM analysis. The I2 state was considered the reference state at zero energy.

Table 1. Kinetics and thermodynamic parameters calculated from the force dependence of transition rates at 10 mM and 10 μM Ca^{2+} concentration

	10 mM Ca^{2+}		10 μM Ca^{2+}	
Transition	$x^{‡}$, nm	$\Delta G^{‡}$, k_BT	$x^{‡}$, nm	$\Delta G^{‡}$, k_BT
M2→I2	3.1 ± 0.6	6.1 ± 1.2	1.2 ± 0.4	6.8 ± 0.7
I2→M2	1.8 ± 1.2	7.4 ± 2.3	3.0 ± 0.8	9.5 ± 1.4
x_{total}, nm	4.9 ± 1.3		4.2 ± 1	
M1→I2	1.9 ± 0.6	7.1 ± 1.2	—	—
I2→M1	6.6 ± 1.2	8.0 ± 2.3	—	—
x_{total}, nm	8.5 ± 1.3		—	

Here $x^{‡}$ is the distance to the transition state for the unfolding and refolding reaction, and x_{total} is the distance between two states. $\Delta G^{‡}$ is the activation energy barrier for the different transitions at 5.5 pN calculated from the rates, using a preexponential factor of 1.2×10^4 Hz. Errors are estimated from fit parameters' uncertainties; k_BT = 2.5 kJ mol^{-1}.

Finally, once the molecule had populated a pathway leading to misfolded states, we analyzed the overall folding rate of NCS-1 as a function of force. At both high (Fig. 5*A*) and low (Fig. 5*B*) calcium concentrations, the probability of observing native folding decreased at lower forces, displaying an essentially linear and positive correlation with force. These results seem puzzling because we would expect lower forces to favor the native state. In fact, the rate for the transition I2−I1 as estimated by HMM analysis increases as the applied tension is reduced (Fig. 5 *C* and *D*), but such an effect is outweighed by the increased lifetime of the misfolded states, as shown in Figs. 3 *B* and *C* and 4*B*.

Discussion

The application of single-molecule techniques has lately proven to be a powerful approach to detect and characterize protein misfolded states (3, 20, 22, 50), and to investigate their link to neurodegenerative diseases (1, 51). Here we have used optical tweezers to study the molecular rearrangements leading to misfolded conformations of the NCS-1 protein. We have shown that the misfolding behavior of NCS-1 can be controlled by

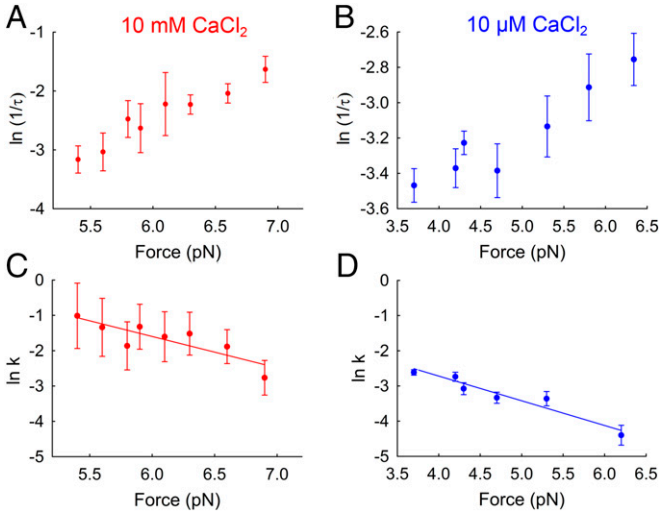

Fig. 5. Occupation of misfolded states slows the overall folding rate of NCS-1. In *A* and *B*, τ is the total time elapsed from the beginning of the force clamp until the protein eventually folds into N (this takes into account also the time spent visiting misfolded states). In *C* and *D*, we plot the force dependence of the rate constants for the I2–I1 transition in 10 mM and 10 μM $CaCl_2$, respectively. The solid line represents fits to the data according to the Bell model. The extrapolated zero-force folding rate at 10 mM $CaCl_2$ is 40 ± 4 s^{-1}, in remarkable agreement with the value of 38 ± 5 s^{-1} that we found performing experiments at higher force (around 10 pN) (39). The folding rate at 10 μM is lowered by a factor of ∼40 (1.1 ± 1.6 s^{-1}), whereas the distance to the transition state is similar at both calcium concentrations (x_f = 3.3 ± 1.0 nm at 10 mM $CaCl_2$; x_f = 2.9 ± 0.4 nm at 10 μM $CaCl_2$).

modulating the relaxation rate of the applied force, a phenomenon previously observed with RNA hairpins (52) but not, to our knowledge, with proteins (16, 21, 40, 53). Precision control over protein folding energy landscapes may find practical applications in the study of molecules that have established links to misfolding diseases. The fate of a protein during folding strictly depends on the topography of its energy landscape. Our results suggest a complicated and rugged energy landscape for NCS-1, with several local maxima and minima that can act as kinetic traps. During folding, nonnative contacts can become accessible before native contacts form (54). If the force is decreased faster than the rate at which nonnative contacts can break, the molecule becomes kinetically trapped in misfolded structures. Mechanical force can then be used to pull out misfolded species from their energy minima and rescue native folding.

Our results add a new layer of complexity to the folding process of NCS-1, revealing a rugged multidimensional folding energy landscape governed by a kinetic partitioning mechanism. The process invariably starts with the folding of the polypeptide chain into the intermediate state I2. From here, it can proceed toward the native state by transiting into intermediate state I1 or, in a calcium-dependent manner, take alternative pathways leading to misfolded states M1 and M2. Two distinct misfolded states have previously been observed in the structurally related two-domain EF-hand protein CaM (21), yet those states appear to be different from the ones observed for NCS-1. First, the modulation of misfolding by calcium has, to the best of our knowledge, not yet been reported for CaM, or for any other protein. Second, for both misfolded states of NCS-1, the C domain is only partially folded, whereas both CaM misfolded states consist of EF hands that are either unfolded or fully folded, although incorrectly paired. The difference in the misfolding mechanisms may be a reflection of the different structural architectures of the two proteins. CaM has a rather symmetrical structure, with a long α-helix separating the two almost identical N and C domains, each binding two Ca^{2+} ions (55). In contrast, NCS-1 is characterized by a certain asymmetry, as the N domain binds only one Ca^{2+} ion, and by significantly more interdomain contacts (38). Despite these differences, the occupation of misfolded states has been shown to slow down the overall folding rates of both NCS-1 and CaM, with a potential impact on their functions (21). Our constant-velocity and constant-force data suggest partial or near-complete folding of the N domain in misfolded states M2 and M1, respectively, and indicate that both the EF2 and EF4 Ca^{2+}-binding sites play important roles in misfolding. The ability of EF2 and EF4 to bind calcium appears to be a prerequisite for wild-type NCS-1 to populate M1 and M2. If either of the two EF hands is disabled, NCS-1 behaves differently. Subsequent to calcium binding to EF3, the EF2 and EF4 sites may compete both for calcium and for successive interaction with a folded EF3. This slows productive folding because native folding requires EF3 to interact with a folded EF4 and hence any nonnative EF2–EF3 contacts need consequently to be broken. We have previously shown how the crosstalk between different EF hands is important for the folding process of NCS-1 (39). Here we report data that highlight the importance of EF-hand crosstalk for the misfolding of NCS-1.

We observed NCS-1 misfolding even at low calcium levels, suggesting a physiological relevance. Intracellular Ca^{2+} levels are tightly regulated in neurons, maintained at 40–100 nM at resting levels and rising to about 1–10 μM under excited conditions (42). However, even under normal conditions, Ca^{2+} concentrations can transiently (seconds to minutes) reach hundreds of micromolars, especially in the vicinity of Ca^{2+} channels (42, 43). When calcium homeostasis fails, the resulting and sustained high concentrations of cytosolic Ca^{2+} can have severe consequences for neurons, including deleterious effects on synaptic function and eventually cell death (44). A hypothesis gaining increasing support in recent years postulates that aging is a result of Ca^{2+} dysregulation (56, 57). Many factors in aging neurons, such as increased release of Ca^{2+} from intracellular stores and increased Ca^{2+} influx through L-type voltage-gated calcium channels, lead to sustained elevation of free Ca^{2+} concentration (56, 58). Moreover, calcium dysregulation has been implicated in the development of major neural disorders such as Alzheimer's disease, BD, and schizophrenia, and drugs that reduce Ca^{2+} signaling activity have in some cases proved successful in alleviating symptoms (59, 60). Interestingly, NCS-1 is highly up-regulated in schizophrenic and BD patients, and substantial evidence suggests that resting and activated levels of Ca^{2+} are elevated in BD (61). Whether NCS-1 is up-regulated to counteract loss of function as a consequence of Ca^{2+}-induced increased misfolding is unknown but might be a highly interesting avenue of research.

Despite both Ca^{2+} homeostasis and protein misfolding being linked to neurodegeneration (5, 59), a direct causation between the two former has been missing. Here, using single-molecule optical tweezers, a putative link has been revealed between Ca^{2+} dysregulation, misfolding, and an NCS protein involved in neurodegenerative disorders. Thus, Ca^{2+} may not only shape the function of the NCS family but also cause its dysfunction in vivo.

Methods

The engineering, expression, and purification of the double-cysteine variants of unmyristoylated human NCS-1, the preparation of protein–DNA chimeric constructs, and the coupling of protein–DNA chimeras to polystyrene beads were performed exactly as described (39, 62). All experiments were performed using a custom-built optical tweezers instrument with a dual-beam laser trap of 840-nm wavelength. Measurements were conducted at ambient temperatures in 10 mM Tris, 250 mM NaCl at pH 7.0 with varying concentrations of $CaCl_2$ in the range 0.5 μM to 10 mM (*SI Methods*).

Changes in contour length associated with (un)folding transitions were estimated by fitting constant-velocity traces to the WLC model, as previously described (16, 39). The thermodynamics and kinetics of the transitions between molecular states I2, M1, and M2 in constant-force measurements were characterized using a HMM algorithm, as previously described (39). The

force dependence of the transition rates was analyzed with the phenomenological Bell model (63) to estimate the position of the barriers and the barriers' heights, using a preexponential factor of 1.2×10^{-4} Hz (39, 49). A total of 84 and 62 extension vs. time traces, from roughly 20 and 10 molecules, were used in our energy landscape reconstruction at 10 mM and 10 μM Ca^{2+}, respectively (*SI Methods*).

ACKNOWLEDGMENTS. We thank Dr. P. T. X. Li for critical comments on the manuscript. P.O.H. and B.B.K. acknowledge the Carlsberg Foundation and the Lundbeck Foundation for financial support. C.C. gratefully acknowledges financial support from Fondazione Cassa di Risparmio di Modena, the European Union (EU) through Marie Curie International Re-Integration Grant 44952, the Italian Ministry of Education, University, and Research (MIUR) Grant 17DPXLNBEK, and partial support from Italian MIUR Basic Research Investment Fund (FIRB) RBPR05JH2P "ITALNANONET." M.R.O. gratefully acknowledges financial support from the Abdus Salam International Centre for Theoretical Physics, of United Nations Educational, Scientific and Cultural Organization (UNESCO), and the International Atomic Energy Agency (IAEA), Programme for Training and Research in Italian Laboratories (TRIL).

1. Chiti F, Dobson CM (2006) Protein misfolding, functional amyloid, and human disease. *Annu Rev Biochem* 75:333–366.
2. Zheng W, Schafer NP, Wolynes PG (2013) Frustration in the energy landscapes of multidomain protein misfolding. *Proc Natl Acad Sci USA* 110(5):1680–1685.
3. Borgia MB, et al. (2011) Single-molecule fluorescence reveals sequence-specific misfolding in multidomain proteins. *Nature* 474(7353):662–665.
4. Hartl FU, Bracher A, Hayer-Hartl M (2011) Molecular chaperones in protein folding and proteostasis. *Nature* 475(7356):324–332.
5. Soto C (2003) Unfolding the role of protein misfolding in neurodegenerative diseases. *Nat Rev Neurosci* 4(1):49–60.
6. Pastore A, Temussi P (2012) Protein aggregation and misfolding: Good or evil? *J Phys Condens Matter* 24(24):244101.
7. Teilum K, et al. (2009) Transient structural distortion of metal-free Cu/Zn superoxide dismutase triggers aberrant oligomerization. *Proc Natl Acad Sci USA* 106(43):18273–18278.
8. Chiti F, Dobson CM (2009) Amyloid formation by globular proteins under native conditions. *Nat Chem Biol* 5(1):15–22.
9. Danielsson J, et al. (2013) Global structural motions from the strain of a single hydrogen bond. *Proc Natl Acad Sci USA* 110(10):3829–3834.
10. Eichner T, Kalverda AP, Thompson GS, Homans SW, Radford SE (2011) Conformational conversion during amyloid formation at atomic resolution. *Mol Cell* 41(2): 161–172.
11. DeMarco ML, Daggett V (2004) From conversion to aggregation: Protofibril formation of the prion protein. *Proc Natl Acad Sci USA* 101(8):2293–2298.
12. Calamai M, Chiti F, Dobson CM (2005) Amyloid fibril formation can proceed from different conformations of a partially unfolded protein. *Biophys J* 89(6):4201–4210.
13. Gianni S, et al. (2010) Structural characterization of a misfolded intermediate populated during the folding process of a PDZ domain. *Nat Struct Mol Biol* 17(12): 1431–1437.
14. Zoldák G, Rief M (2013) Force as a single molecule probe of multidimensional protein energy landscapes. *Curr Opin Struct Biol* 23(1):48–57.
15. Moffitt JR, Chemla YR, Smith SB, Bustamante C (2008) Recent advances in optical tweezers. *Annu Rev Biochem* 77:205–228.
16. Cecconi C, Shank EA, Bustamante C, Marqusee S (2005) Direct observation of the three-state folding of a single protein molecule. *Science* 309(5743):2057–2060.
17. Heidarsson PO, Naqvi MM, Sonar P, Valpapuram I, Cecconi C (2013) Conformational dynamics of single protein molecules studied by direct mechanical manipulation. *Advances in Protein Chemistry and Structural Biology*, ed Tatyana K-C (Academic, New York), Vol 92, pp 93–133.
18. Schlierf M, Yew ZT, Rief M, Paci E (2010) Complex unfolding kinetics of single-domain proteins in the presence of force. *Biophys J* 99(5):1620–1627.
19. Mashaghi A, et al. (2013) Reshaping of the conformational search of a protein by the chaperone trigger factor. *Nature* 500(7460):98–101.
20. Yu H, et al. (2012) Direct observation of multiple misfolding pathways in a single prion protein molecule. *Proc Natl Acad Sci USA* 109(14):5283–5288.
21. Stigler J, Ziegler F, Gieseke A, Gebhardt JC, Rief M (2011) The complex folding network of single calmodulin molecules. *Science* 334(6055):512–516.
22. Xi Z, Gao Y, Sirinakis G, Guo H, Zhang Y (2012) Single-molecule observation of helix staggering, sliding, and coiled coil misfolding. *Proc Natl Acad Sci USA* 109(15): 5711–5716.
23. Chazin WJ (2011) Relating form and function of EF-hand calcium binding proteins. *Acc Chem Res* 44(3):171–179.
24. Weiss JL, Hui H, Burgoyne RD (2010) Neuronal calcium sensor-1 regulation of calcium channels, secretion, and neuronal outgrowth. *Cell Mol Neurobiol* 30(8):1283–1292.
25. Reyes-Bermudez A, Miller DJ, Sprungala S (2012) The neuronal calcium sensor protein Acrocalcin: A potential target of calmodulin regulation during development in the coral *Acropora millepora*. *PLoS ONE* 7(12):e51689.
26. Gomez M, et al. (2001) Ca2+ signaling via the neuronal calcium sensor-1 regulates associative learning and memory in *C. elegans*. *Neuron* 30(1):241–248.
27. Saab BJ, et al. (2009) NCS-1 in the dentate gyrus promotes exploration, synaptic plasticity, and rapid acquisition of spatial memory. *Neuron* 63(5):643–656.
28. Pongs O, et al. (1993) Frequenin—A novel calcium-binding protein that modulates synaptic efficacy in the *Drosophila* nervous system. *Neuron* 11(1):15–28.
29. McFerran BW, Graham ME, Burgoyne RD (1998) Neuronal Ca2+ sensor 1, the mammalian homologue of frequenin, is expressed in chromaffin and PC12 cells and regulates neurosecretion from dense-core granules. *J Biol Chem* 273(35):22768–22772.
30. Navarro G, et al. (2012) NCS-1 associates with adenosine A(2A) receptors and modulates receptor function. *Front Mol Neurosci* 5(5):53.
31. Kabbani N, Negyessy L, Lin R, Goldman-Rakic P, Levenson R (2002) Interaction with neuronal calcium sensor NCS-1 mediates desensitization of the D2 dopamine receptor. *J Neurosci* 22(19):8476–8486.
32. Koh PO, et al. (2003) Up-regulation of neuronal calcium sensor-1 (NCS-1) in the prefrontal cortex of schizophrenic and bipolar patients. *Proc Natl Acad Sci USA* 100(1): 313–317.
33. Piton A, et al.; S2D team (2008) Mutations in the calcium-related gene IL1RAPL1 are associated with autism. *Hum Mol Genet* 17(24):3965–3974.
34. Handley MT, Lian LY, Haynes LP, Burgoyne RD (2010) Structural and functional deficits in a neuronal calcium sensor-1 mutant identified in a case of autistic spectrum disorder. *PLoS ONE* 5(5):e10534.
35. Aravind P, et al. (2008) Regulatory and structural EF-hand motifs of neuronal calcium sensor-1: Mg 2+ modulates Ca 2+ binding, Ca 2+ -induced conformational changes, and equilibrium unfolding transitions. *J Mol Biol* 376(4):1100–1115.
36. Stigler J, Rief M (2012) Calcium-dependent folding of single calmodulin molecules. *Proc Natl Acad Sci USA* 109(44):17814–17819.
37. Mukherjee S, Mohan PM, Kuchroo K, Chary KV (2007) Energetics of the native energy landscape of a two-domain calcium sensor protein: Distinct folding features of the two domains. *Biochemistry* 46(35):9911–9919.
38. Heidarsson PO, et al. (2012) The C-terminal tail of human neuronal calcium sensor 1 regulates the conformational stability of the Ca^{2+}- activated state. *J Mol Biol* 417(1-2): 51–64.
39. Heidarsson PO, et al. (2013) Single-molecule folding mechanism of an EF-hand neuronal calcium sensor. *Structure* 21(10):1812–1821.
40. Heidarsson PO, et al. (2012) A highly compliant protein native state with a spontaneous-like mechanical unfolding pathway. *J Am Chem Soc* 134(41):17068–17075.
41. Bustamante C, Marko JF, Siggia ED, Smith S (1994) Entropic elasticity of lambda-phage DNA. *Science* 265(5178):1599–1600.
42. Augustine GJ, Santamaria F, Tanaka K (2003) Local calcium signaling in neurons. *Neuron* 40(2):331–346.
43. Burgoyne RD (2007) Neuronal calcium sensor proteins: Generating diversity in neuronal Ca2+ signalling. *Nat Rev Neurosci* 8(3):182–193.
44. Seaton G, Hogg EL, Jo J, Whitcomb DJ, Cho K (2011) Sensing change: The emerging role of calcium sensors in neuronal disease. *Semin Cell Dev Biol* 22(5):530–535.
45. Chodera JD, et al. (2011) Bayesian hidden Markov model analysis of single-molecule force spectroscopy: Characterizing kinetics under measurement uncertainty. arXiv: 1108:1430.
46. McKinney SA, Joo C, Ha T (2006) Analysis of single-molecule FRET trajectories using hidden Markov modeling. *Biophys J* 91(5):1941–1951.
47. Gao Y, Sirinakis G, Zhang Y (2011) Highly anisotropic stability and folding kinetics of a single coiled coil protein under mechanical tension. *J Am Chem Soc* 133(32): 12749–12757.
48. Bell GI (1978) Models for the specific adhesion of cells to cells. *Science* 200(4342): 618–627.
49. Gebhardt JC, Bornschlögl T, Rief M (2010) Full distance-resolved folding energy landscape of one single protein molecule. *Proc Natl Acad Sci USA* 107(5):2013–2018.
50. Cremades N, et al. (2012) Direct observation of the interconversion of normal and toxic forms of α-synuclein. *Cell* 149(5):1048–1059.
51. Dobson CM (2003) Protein folding and misfolding. *Nature* 426(6968):884–890.
52. Li PT, Bustamante C, Tinoco I, Jr (2007) Real-time control of the energy landscape by force directs the folding of RNA molecules. *Proc Natl Acad Sci USA* 104(17):7039–7044.
53. Shank EA, Cecconi C, Dill JW, Marqusee S, Bustamante C (2010) The folding cooperativity of a protein is controlled by its chain topology. *Nature* 465(7298):637–640.
54. Linse S, Linse B (2007) Protein folding through kinetic discrimination. *J Am Chem Soc* 129(27):8481–8486.
55. Chattopadhyaya R, Meador WE, Means AR, Quiocho FA (1992) Calmodulin structure refined at 1.7 Å resolution. *J Mol Biol* 228(4):1177–1192.
56. Oliveira AM, Bading H (2011) Calcium signaling in cognition and aging-dependent cognitive decline. *Biofactors* 37(3):168–174.
57. Khachaturian ZS (1989) The role of calcium regulation in brain aging: Reexamination of a hypothesis. *Aging (Milano)* 1(1):17–34.
58. Toescu EC, Vreugdenhil M (2010) Calcium and normal brain ageing. *Cell Calcium* 47(2):158–164.
59. Berridge MJ (2012) Calcium signalling remodelling and disease. *Biochem Soc Trans* 40(2):297–309.
60. Berridge MJ (2013) Dysregulation of neural calcium signaling in Alzheimer disease, bipolar disorder and schizophrenia. *Prion* 7(1):2–13.
61. Warsh JJ, Andreopoulos S, Li PP (2004) Role of intracellular calcium signaling in the pathophysiology and pharmacotherapy of bipolar disorder: Current status. *Clin Neurosci Res* 4(3-4):201–213.
62. Cecconi C, Shank EA, Dahlquist FW, Marqusee S, Bustamante C (2008) Protein-DNA chimeras for single molecule mechanical folding studies with the optical tweezers. *Eur Biophys J* 37(6):729–738.
63. Liphardt J, Onoa B, Smith SB, Tinoco I, Jr, Bustamante C (2001) Reversible unfolding of single RNA molecules by mechanical force. *Science* 292(5517):733–737.

Supporting Information

Heidarsson et al. 10.1073/pnas.1401065111

SI Methods

Experimental Procedures. The double-cysteine construct of NCS-1, placing cysteine residues at positions 4 and 188, was engineered using a pseudowild-type pET-16b expression plasmid (with Cys38 replaced by serine), by standard genetic techniques. This variant has previously been shown to have comparable stability, structure, and calcium-binding properties to the wild-type protein (1). The *Escherichia coli* strain BL21 (DE3) was used to express unmyristoylated human NCS-1 and was grown at 37 °C in Luria–Bertani medium.

Individual proteins were manipulated by means of ∼500 bp DNA molecules covalently attached to exposed cysteine residues through a disulfide bond. One DNA handle bears a 5′ digoxigenin moiety that interacts with an optically trapped 3.1-μm polystyrene bead coated with anti-digoxigenin antibodies (Spherotec), while the other handle bears a 5′ biotin moiety that interacts with a 2.18-μm streptavidin-coated bead (Spherotech) held in place at the end of a pipette by suction (2). The force applied to the molecule was varied by moving the micropipette toward or away from the optical trap by means of a piezoelectric flexure stage (MAX311/M, Thorlabs). The applied force was determined by measuring the change in light momentum of the laser beams leaving the trap, whereas changes in the extension of the molecule were determined by measuring the distance between the two beads (3). Force vs. extension traces were collected at constant speeds from 5 to 1,000 $nm{\cdot}s^{-1}$. During constant-velocity experiments, data were recorded at a rate of 40 Hz. In constant-force experiments, the force was kept constant through a force-feedback mechanism, where the average force was measured and compared with the set-point force value every 1 ms. Differences between forces were compensated for by movement of the micropipette. In constant-force experiments, data were recorded at a rate of 100 Hz.

Hidden Markov Model. Hidden Markov model (HMM) algorithms have recently replaced threshold-based methods as the tool of choice to study the time series obtained in single-molecule experiments (4). Originally developed during the 1960s by mathematicians and engineers interested in artificial intelligence, HMM is based upon the idea of modeling the system of interest as a Markov chain that is hidden in the sense that the state of the system is not directly accessible: Each state, however, emits a signal according to a discrete or continuous distribution. The (time-independent) transition matrix characterizing the Markov process as well as the parameters of the signal emission distributions may be inferred from a sequence of observations by applying an iterative procedure introduced by Baum and Petrie (5). We refer to the excellent tutorial written by Rabiner (6) for theoretical and practical details about this statistical method. Here we just outline the various passages from the data to the kinetic and thermodynamic parameters reported in Table 1.

Each extension vs. time trace is individually analyzed by means of a four-state (I2, M1, M2, N) HMM routine where we assume that the end-to-end extension associated with each state is normally distributed. The logarithm of the reconstructed transition probability matrix, divided by the time interval between two consecutive measurements, yields the transition rates among the states of our Markovian model. By means of the simplified Kramers–Bell theory derived, for instance, in ref. 7, we can estimate from the force dependence of the rates the position of the barriers and the free energy of the states. An estimation of the barriers' heights requires the knowledge of the preexponential factor, which we cannot measure directly with our experimental apparatus. We adopt, therefore, the value $1.2 \times 10^{-4}\ s^{-1}$, which has been measured in an experiment with a similar setup as ours, albeit using a different protein (8).

1. Heidarsson PO, et al. (2013) Single-molecule folding mechanism of an EF-hand neuronal calcium sensor. *Structure* 21(10):1812–1821.
2. Cecconi C, Shank EA, Dahlquist FW, Marqusee S, Bustamante C (2008) Protein-DNA chimeras for single molecule mechanical folding studies with the optical tweezers. *Eur Biophys J* 37(6):729–738.
3. Smith SB, Cui Y, Bustamante C (2003) Optical-trap force transducer that operates by direct measurement of light momentum. *Methods Enzymol* 361:134–162.
4. McKinney SA, Joo C, Ha T (2006) Analysis of single-molecule FRET trajectories using hidden Markov modeling. *Biophys J* 91(5):1941–1951.
5. Baum LE, Petrie T (1966) Statistical inference for probabilistic functions of finite state Markov chains. *Ann Math Stat* 37(6):1554–1563.
6. Rabiner LR (1989) A tutorial on hidden Markov models and selected applications in speech recognition. *Proc IEEE* 77(2):257–286.
7. Mossa A, Manosas M, Forns N, Huguet JM, Ritort F (2009) Dynamic force spectroscopy of DNA hairpins: I. Force kinetics and free energy landscapes. *J Stat Mech* 2009(2): P02060.
8. Gebhardt JCM, Bornschlögl T, Rief M (2010) Full distance-resolved folding energy landscape of one single protein molecule. *Proc Natl Acad Sci USA* 107(5):2013–2018.

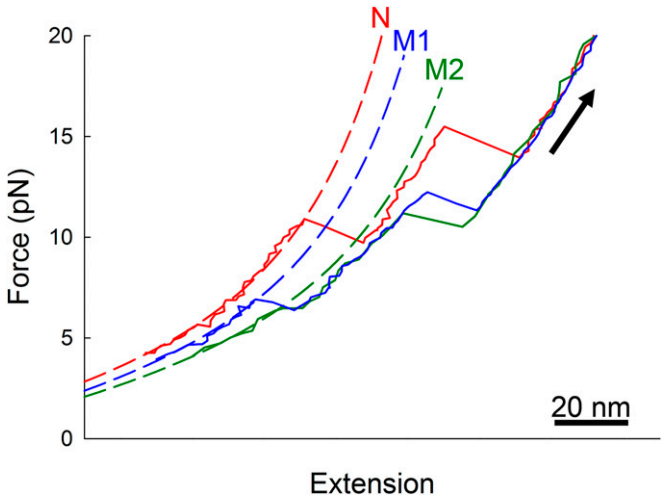

Fig. S1. Unfolding trajectories of different NCS-1 molecular states. The native state (N) of NCS-1 unfolds through two high-force transitions corresponding to the mechanical denaturation of the N and C domains, respectively (red trace). In contrast, misfolded states M1 (blue) and M2 (green) display drastically reduced mechanical stability. Dashed lines are worm-like-chain fits to the data. The arrow indicates the pulling direction.

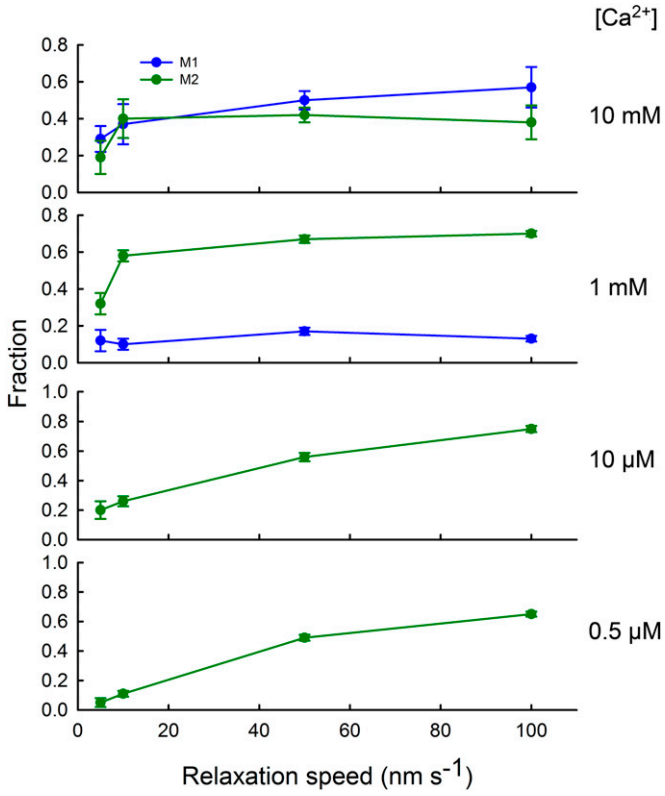

Fig. S2. Occupation probability of misfolded states M1 and M2 as a function of relaxation speed and Ca^{2+} concentration. The M1 state is observed only at high Ca^{2+} concentrations. The M2 state is observed at all experimental conditions.

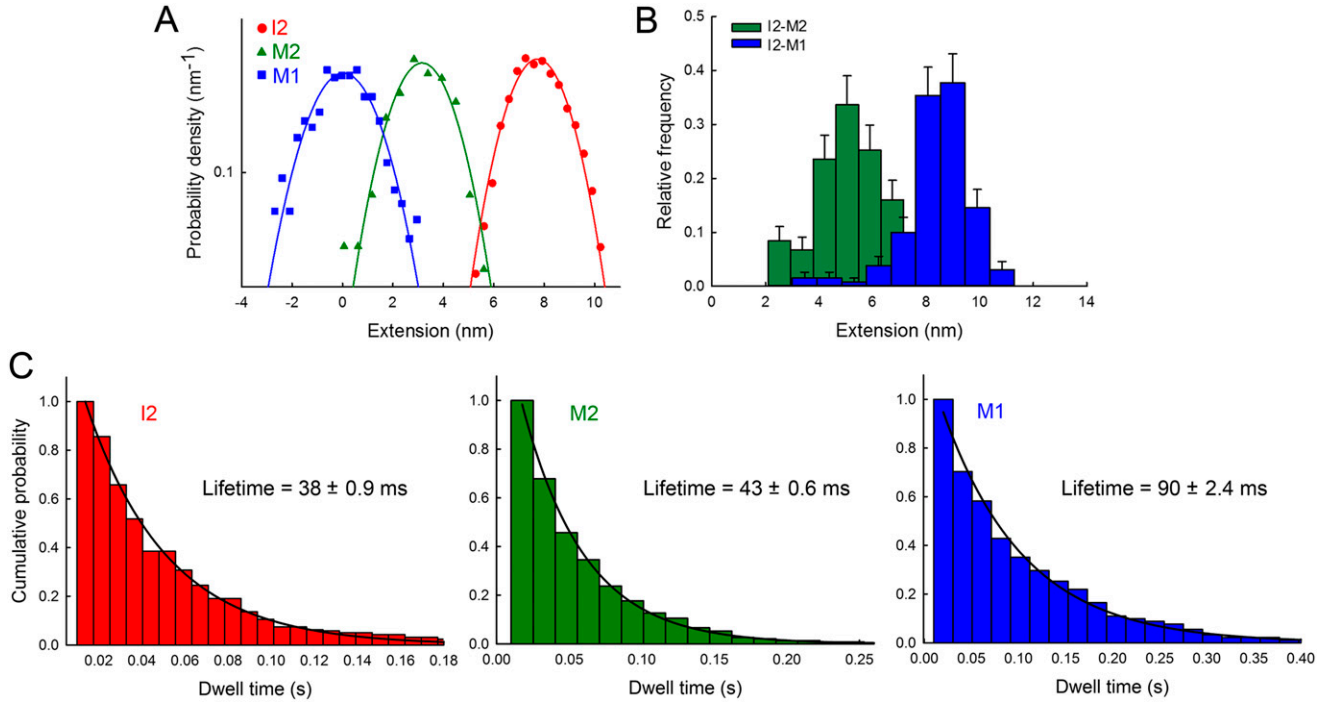

Fig. S3. Extension and lifetimes of NCS-1 misfolded states at 10 mM Ca^{2+}. (*A*) Probability density distributions of the extension of the molecular states I2 (red), M1 (blue), and M2 (green) identified by the HMM algorithm in an extension vs. time trace acquired at 5.9 pN. The distributions were fitted to Gaussian functions, which estimated changes in extension of 4.5 ± 1.8 nm for the I2–M2 transition and of 7.7 ± 1.8 nm for the I2–M1 transition. (*B*) Distribution of the changes in extension for the I2–M2 and I2–M1 transition, calculated using all extension vs. time traces. The medians of these distributions are 5.1 ± 2 nm and 8.6 ± 2 nm, respectively. (*C*) Dwell time distributions of I2 (red), M2 (green), and M1 (blue) at 6.2 pN. The distributions could be well fitted to single-exponential functions.

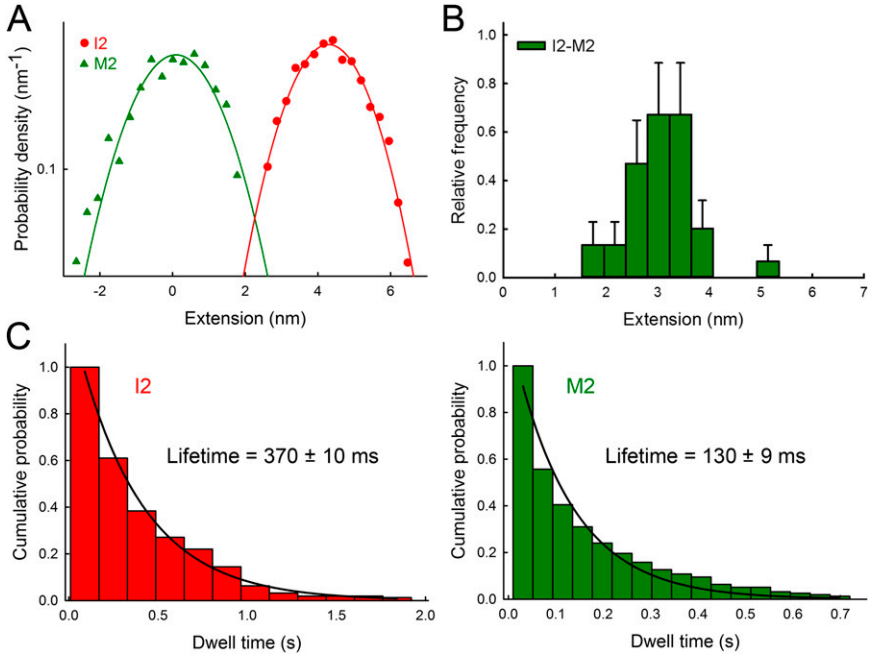

Fig. S4. Extension and lifetimes of NCS-1 misfolded states at 10 μM Ca^{2+}. (*A*) Probability density distributions of the extension of the molecular states I2 (red) and M2 (green) identified by HMM analysis in an extension vs. time trace acquired at 4.7 pN. The distributions were fitted to Gaussian functions, which estimated a change in extension of 4.2 ± 1.6 nm for the I2–M2 transition. (*B*) Distribution of the changes in extension for the I2–M2 transition, calculated using all extension vs. time traces. The median of this distribution is 3.3 ± 1.4 nm. (*C*) Dwell time distributions of I2 (red) and M2 (green) at 3.7 pN. The distributions could be well fitted to single-exponential functions.

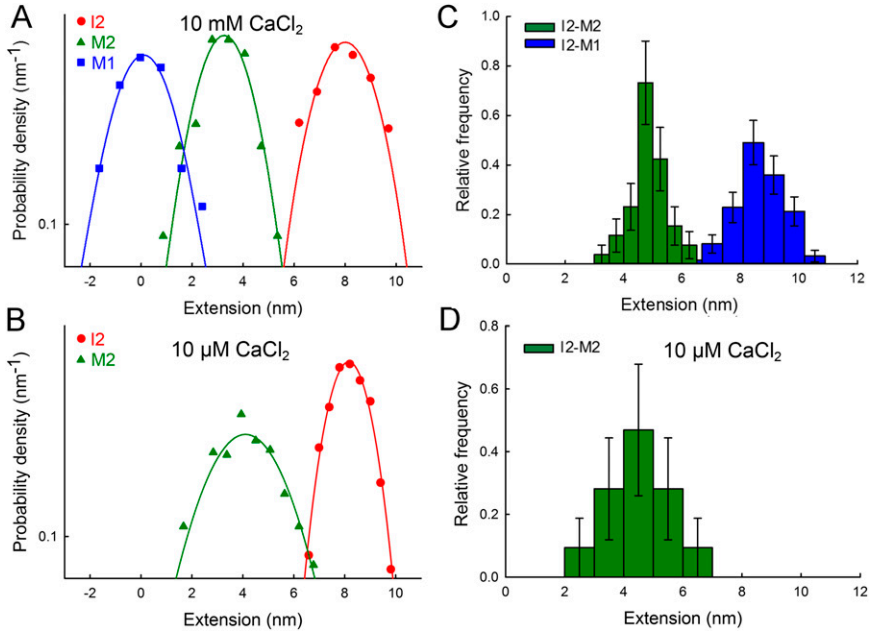

Fig. S5. Comparative extension analysis of NCS-1 misfolded states in the same force range at high and low Ca^{2+}. *A* and *B* show probability density distributions of the extensions of the molecular states I2 (red), M1 (blue), and M2 (green) identified by HMM analysis in extension vs. time traces acquired at 5.8 pN in either 10 mM $CaCl_2$ (*A*) or 10 μM $CaCl_2$ (*B*). The distributions were fitted to Gaussian functions, which estimated a change in extension of 4.8 ± 2.0 nm and 4.2 ± 1.8 nm for the I2−M2 transition at 10 mM and 10 μM $CaCl_2$, respectively, and 8.0 ± 2.0 nm for the I2−M1 transition at 10 mM $CaCl_2$. *C* and *D* show distribution of the changes in extension for the I2−M1 and I2−M2 transitions, calculated using extension vs. time traces in the force range 5.4–6.2 pN at both 10 mM and 10 μM $CaCl_2$. The median of the distribution for the I2−M2 transition is 4.8 ± 1.0 nm and 4.5 ± 1.0 nm at 10 mM and 10 μM $CaCl_2$, respectively, and that of the distribution for the I2−M1 transition is 8.6 ± 2.0 nm at 10 mM $CaCl_2$.

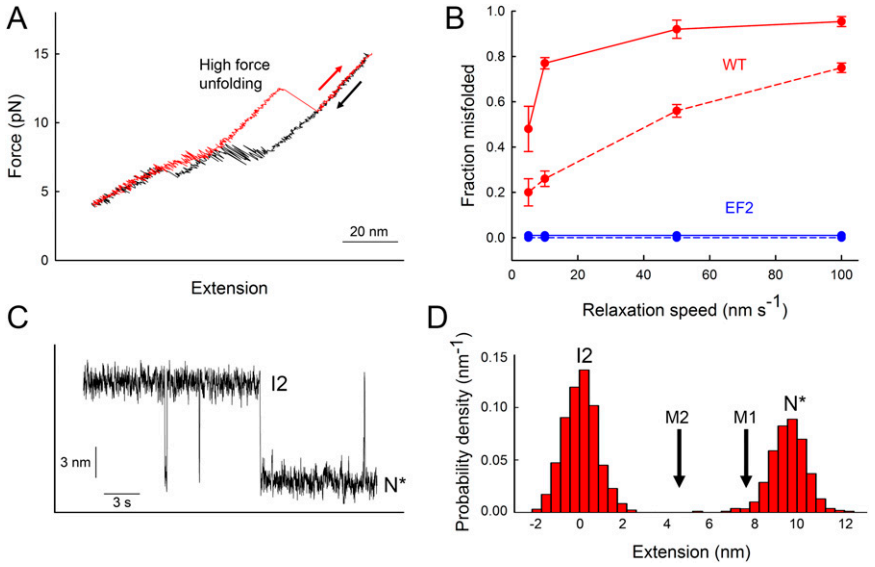

Fig. S6. Folding behavior of the NCS-1^{EF2} and NCS-1^{EF4} variants. (*A*) Force vs. extension trace for NCS-1^{EF2} at 10 mM $CaCl_2$ and 100 nm·s^{-1}. In this variant, the C domain always folds correctly as evident from the high-force unfolding transition (average unfolding force of 13.7 ± 1.0 pN), signifying a natively folded domain (1). Color-coded arrows indicate pulling direction. (*B*) Fraction of relaxation traces in which the C domain misfolds in constant-velocity experiments as a function of relaxation speed for NCS-1 (red) and NCS-1^{EF2} (blue). Data acquired in both 10 mM (solid lines; 230 events, six molecules) and 10 μM (dashed lines; 180 events, three molecules) $CaCl_2$ are shown. The C domain of the NCS-1^{EF2} variant does not misfold at any calcium concentration or relaxation speed. Data for WT NCS-1 is from Fig. 1. (*C*) Extension vs. time traces for NCS-1^{EF4} at 5.4 pN and 10 mM $CaCl_2$. The molecule shows only fluctuations between I2 and a nonnative folded state (N*) with a change in extension that is significantly larger than those associated with the M1 and M2 states (five molecules). Very similar results were obtained at 10 μM $CaCl_2$ (four molecules). (*D*) Probability density distribution of the extension values in the extension-time trace in *C*. Two main populations cluster around 0 nm and ∼9.5 nm. The expected average positions of the two misfolded states are indicated.